

# Cassini-oval description of the multidimensional potential energy surface for $^{236}\text{U}$ : Role of octupole deformation and calculation of the most probable fission path

K. Okada,<sup>1</sup> T. Wada ,<sup>1</sup> R. Capote,<sup>2</sup> and N. Carjan<sup>3,4,5,\*</sup>

<sup>1</sup>*Department of Pure and Applied Physics, Kansai University, 564-8680 Suita, Osaka, Japan*

<sup>2</sup>*NAPC–Nuclear Data Section, International Atomic Energy Agency, 1400 Vienna, Austria*

<sup>3</sup>*Joint Institute for Nuclear Research, 141980 Dubna, Moscow Region, Russia*

<sup>4</sup>*Centre d'Etudes Nucleaires de Bordeaux-Gradignan, UMR 5797, CNRS/IN2P3-University Bordeaux I, BP 120, 33175 Gradignan Cedex, France*

<sup>5</sup>*Horia Hulubei - National Institute for Nuclear Physics and Engineering, P.O.Box MG-6, RO-76900, Bucharest, Romania*



(Received 5 September 2022; accepted 17 February 2023; published 20 March 2023)

Multidimensional potential energy surfaces (PES) are calculated using the microscopic-macroscopic approach. The nuclear shapes are described by Cassinian ovals generalized by the inclusion of  $\alpha_1$ ,  $\alpha_3$ , and  $\alpha_4$  shape parameters in addition to the main fission coordinate  $\alpha$ . The influence of the octupole deformation ( $\alpha_3$ ) on the PES is studied in the case of the nuclear fission of  $^{236}\text{U}$ . It is found that  $\alpha_3$  plays an important role in the last stage of the fission process; for instance, it lowers the third minimum and the third barrier. Two methods to calculate the static fission path are investigated. They are found to be consistent in the sense that they lead to the same fission barrier. In certain subspaces, the least energy paths from the ground state to scission present discontinuities around one of the saddles. They are caused by sharp changes in the nuclear shapes involved occurring without a change in energy. Such transitions are smoothed out by the principle of stationary action, which transforms a discontinuous path into a continuous one. Finally, various macroscopic models have been employed in order to study their influence on the energies and positions of the saddles and the minima.

DOI: [10.1103/PhysRevC.107.034608](https://doi.org/10.1103/PhysRevC.107.034608)

## I. INTRODUCTION

The recent discussions of the role of the octupole degree of freedom in the formation of the fission fragments brought some freshness to the old field of nuclear fission. In particular, it was shown [1] that in the super-heavy elements (SHE) region, inclusion of  $\alpha_3$  produces a spectacular change from symmetric to asymmetric fission. In Ref. [2]  $\alpha_3$  was brought to the highest level of importance: it is the main reason for the asymmetric fission of actinides removing  $^{132}\text{Sn}$  from the bench. New experimental information on low-energy fission of neutron-deficient pre-actinides [3] indicates a large deformation of the fragments at scission that can be explained, using a stationary energy density functional approach [4], by a quadrupole-octupole correlation with a large octupole component. If  $\alpha_3$  is important at scission, it could also matter before. For instance, it could modify the fission barriers affecting the calculation of the fission cross sections.

The importance of nuclear octupolar vibrations has been also highlighted in nuclear structure studies of actinide nuclei. The energies of excited states of the ground-state rotational band of even-even actinides below 500 keV are well described by a rigid rotor model, however, the first excited vibrational band in actinides usually corresponds to octupolar vibrations of the deformed core [5–9]. In  $^{238}\text{U}$  for instance, negative parity levels built on top of the band head at 680 keV are

interpreted as an octupolar vibrational band, which is the lowest excited rotational band above the ground state rotational band.

The octupolar rotational band, built on the vibrational octupolar band head for even-even targets, needs to be considered in the fast neutron inelastic scattering studies on even-even actinides. Those excited states with excitation energies from 400 up to 1200 keV are very strongly coupled to the ground state band in fast neutron scattering, and correspond to neutron energies with a maximum flux of fission neutrons which are critical for a proper description of fast nuclear reactors. Such a vibrational-rotational description within a coupled-channels approach [10] has been widely used to describe scattering data [11–15].

Hence, octupolar vibrations in actinides are a well-established phenomenon which is important both for low- and high-amplitude vibrations.

It is therefore useful to study the effect of the octupole deformation on the fission path and this is the main purpose of the present work. We choose the particular case of  $^{236}\text{U}$  fissioning compound, having in mind the reaction  $^{235}\text{U}(n_{th}, f)$ .

To achieve this goal the microscopic-macroscopic approach proposed by Strutinsky [16] is employed to obtain the potential energy surface (PES) as a function of several shape parameters. Not doing self-consistent calculations, it is important to use a well-converged shape parametrization suited for extremely elongated nuclei since we need a reliable description of the last stage of the fission process. Such parametrization is the generalization of the Cassini ovals [17]

\*carjan@theory.nipne.ro

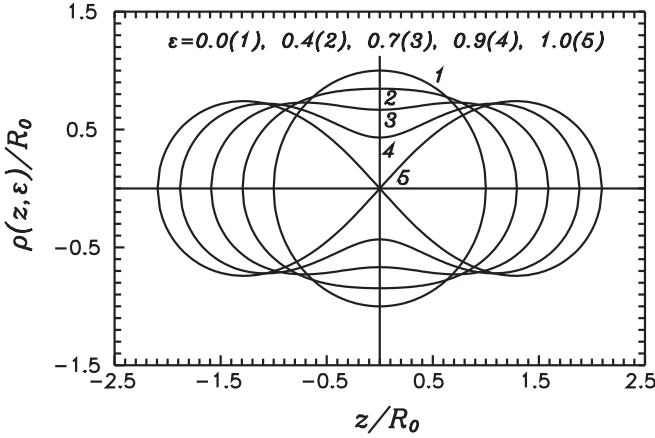


FIG. 1. Pure Cassini ovals that conserve the volume at five values of their deformation  $\varepsilon$ .

because one of the basic lines (i.e., before multipolar expansion) corresponds to a zero-neck scission configuration (see further the discussion of Fig. 1). In the present study, we use four deformation parameters ( $\alpha$ ,  $\alpha_1$ ,  $\alpha_3$ , and  $\alpha_4$ ) to explore the PES from a spherical nucleus to the scission configuration for the first time. In Ref. [17] only two parameters were used: mass asymmetry ( $\alpha_1$ ) and elongation ( $\alpha$ ). In Refs. [18,19] the calculations were restricted to a narrow deformation region around the scission line.

Although the generalized Cassini ovals are the most efficient shape parametrization when the fissioning nucleus approaches the scission line, the combined role of neck and mass-asymmetry degrees of freedom have been emphasized many times in the past. References [20–26] represent just a few examples.

For calculation of fission observables or for applications it is necessary to localize the most probable fission path on the PES, in particular the minima (isomers) and maxima (barriers). Two static methods are used to determine the most probable fission path: 1) minimization of the potential energy of deformation as a function of the main fission coordinate, and 2) search for the path in the two-dimensional deformation space (obtained from the four-dimensional space by minimization on the other two deformations) that leads to the minimum value of the action integral.

## II. FORMALISM

The microscopic-macroscopic approach [27] is used to calculate the total deformation energy as a function of the nuclear shape

$$E_{\text{def}}(\text{shape}) = E_{\text{def}}^{\text{LD}}(\text{shape}) + \delta E(\text{shape}) \quad (1)$$

with

$$\delta E = \sum_{n,p} [\delta E_{\text{shell}}^{(n,p)} + \delta E_{\text{pair}}^{(n,p)}]. \quad (2)$$

The summation in Eq. (2) is carried out over the protons ( $p$ ) and neutrons ( $n$ ).

The microscopic shell and pairing corrections are calculated with a Woods-Saxon-type potential suitable for nuclear shapes with pronounced neck [28]. The parameters are taken from [29]. Details on the numerical calculation of the single-particle energies are given in the Appendix.

The  $\delta E_{\text{shell}}$  was calculated by the Strutinsky method as the difference between the sum of single-particle energies of occupied states and the Strutinsky averaged quantity. The  $\delta E_{\text{pair}}$  was evaluated in Bardeen-Cooper-Schrieffer (BCS) approximation as the difference between the calculated pairing energy and the Strutinsky averaged quantity. The pairing strength was taken variable as recommended by Moller and Nix [30].

The  $E_{\text{def}}^{\text{LD}}$  in Eq. (1) is the macroscopic liquid-drop deformation energy

$$E_{\text{def}}^{\text{LD}} = E_{\text{surf}}^{(0)} \{B_{\text{surf}}(\text{shape}) - 1 + 2x_{\text{LD}} [B_{\text{Coul}}(\text{shape}) - 1]\},$$

where  $B_{\text{surf}}$  and  $B_{\text{Coul}}$  are the ratios of deformation dependent surface and Coulomb energies to those for the spherical shape:  $E_{\text{surf}}^{(0)} = 4\pi R_0^2 \Omega$  and  $E_{\text{Coul}}^{(0)} = 3/5(Ze)^2/R_0$ . It turns out that the zero energy is the energy of a spherical liquid drop.  $x_{\text{LD}}$  is the fissility parameter of a nuclear liquid drop,  $x_{\text{LD}} \equiv E_{\text{Coul}}^{(0)}/2E_{\text{surf}}^{(0)}$ . The parameters are taken from [31].

A convenient orthogonal system to describe the shape of a fissioning nucleus is the lemniscate coordinate system  $(R, x)$  [17,32]. In this parametrization, some (scaled) cylindrical coordinates  $\{\bar{\rho}, \bar{z}\}$  are related to the lemniscate coordinates  $\{R, x\}$  by the equations

$$\begin{aligned} \bar{\rho} &= \frac{1}{\sqrt{2}} \sqrt{p(x) - R^2(2x^2 - 1) - s}, \\ \bar{z} &= \frac{\text{sign}(x)}{\sqrt{2}} \sqrt{p(x) + R^2(2x^2 - 1) + s}, \\ p^2(x) &\equiv R^4 + 2sR^2(2x^2 - 1) + s^2, \\ 0 &\leq R \leq \infty, \quad -1 \leq x \leq 1. \end{aligned} \quad (3)$$

In Eq. (3)  $s \equiv \varepsilon R_0^2$  is the squared distance between the focus of Cassinian ovals and the origin of coordinates.  $R_0$  is the radius of the spherical nucleus.

The deviation of the nuclear surface from pure Cassini ovals is defined by expansion of  $R(x)$  in a series of Legendre polynomials  $P_n(x)$ ,

$$R(x) = R_\varepsilon \left[ 1 + \sum_n \alpha_n P_n(x) \right]. \quad (4)$$

This expansion converges rapidly since the basic lines  $R(x) = R_\varepsilon = \text{const}$  represent a sequence of shapes (Cassini ovals) that surprisingly resemble the sequence of shapes of a fissioning nucleus, as can be noticed in Fig. 1.

The cylindrical coordinates  $\{\rho, z\}$  are related to  $\{\bar{\rho}, \bar{z}\}$  by

$$\rho \equiv \bar{\rho}/c, \quad z \equiv (\bar{z} - \bar{z}_{\text{c.m.}})/c, \quad (5)$$

where  $\bar{z}_{\text{c.m.}}$  is the  $z$  coordinate of the center of mass of Cassini ovaloid (4). The constant  $c$  is introduced in order to insure that the volume of the ovaloid is equal to the volume of the spherical nucleus.

Instead of the elongation parameter  $\varepsilon$ , it is convenient to introduce another parameter,  $\alpha$  so that at  $\alpha = 1$  the neck radius

is zero for any values of all other deformation parameters  $\alpha_n$ ,

$$\varepsilon = \frac{\alpha - 1}{4} \left[ \left( 1 + \sum_n \alpha_n \right)^2 + \left( 1 + \sum_n (-1)^n \alpha_n \right)^2 \right] + \frac{\alpha + 1}{2} \left[ 1 + \sum_n (-1)^n \alpha_{2n} (2n - 1)!! / (2^n n!) \right]^2. \quad (6)$$

So we consider  $\alpha$  to be the main fission coordinate. It was demonstrated [33] that even a one-dimensional family of Cassinian shapes,  $\{\alpha = 0.98, \alpha_1\}$  is very close to the optimal scission shapes [34].

For fundamental studies or applications, it is necessary to locate the extreme points on the multidimensional PES, i.e., the minima and the saddles. It is also useful to know the most probable scission configuration where the neck connecting the nascent fragments ruptures. It is at this configuration that the fission fragment properties, such as masses and kinetic energies, are determined. In other words, we need to find the fission path that connects these points and the values of the deformation energy along it, that is usually called the fission barrier. For this we use here two methods:

(1) along the main fission coordinate  $\alpha$ , we minimize the deformation energy with respect to all other deformations ( $\alpha_1, \alpha_3$ , and  $\alpha_4$ );

(2) we find the path  $L$  that minimizes the action integral  $S(L)$  between two points on the PES, usually between the ground state and the outer turning point. It is the path followed by a classical system in the inverted potential.

As mentioned in the Introduction, this path of minimum action is compared with the path of minimum values of  $E_{\text{def}}$  as a function of  $\alpha$ . For this we need to take a constant (any value) inertia. Only in this situation the two methods are equivalent: the particle moves along the bottom of the potential valley.

Dynamical effects that may modify this path (such as a coordinate-dependent inertia) are not included in the present study. On one side they are not reasonably well known and on the other side all tabulated fission barriers, calculated with microscopic self-consistent or microscopic macroscopic models, are static [35–41]. They are used to compare with directly measured barrier heights (for fertile nuclei) or deduced from measurements of fission cross sections (for fissile nuclei) [42–44]. In fact, as a next step, we are planning to extend our calculations to series of actinide nuclei and confront them with “experimental” values and values from other theoretical approaches.

The action integral along a path  $L$  in the deformation space is given by

$$S(L) = 2^{3/2} \hbar^{-1} B^{1/2} \int_{l_1}^{l_2} [E_{\text{def}}(l) - E]^{1/2} dl. \quad (7)$$

$E$  is the energy of the fissioning nucleus. In the case of spontaneous fission, it is the energy of the ground state.  $B$  is taken equal to the reduced mass for symmetric division ( $= 59$ ). As in most applications to nuclear fission, Eq. (8) is calculated in a plane defined by two of the deformation coordinates ( $\alpha_k, \alpha$ ) on a PES minimized with respect to the rest of them.

The minimization of the action integral is done by the von Ritz method. We rotate the  $(\alpha_k, \alpha)$  plane till the line

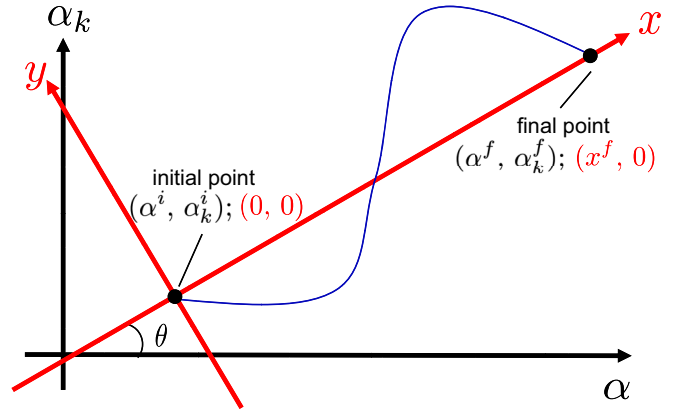


FIG. 2. Coordinate transformation used in the von Ritz method.

connecting  $l_1$  and  $l_2$  becomes the abscissa and choose the initial point as origin (see Fig. 2). The corresponding transformation writes

$$\begin{pmatrix} \alpha - \alpha^i \\ \alpha_k - \alpha_k^i \end{pmatrix} = \begin{pmatrix} \cos \theta & -\sin \theta \\ \sin \theta & \cos \theta \end{pmatrix} \begin{pmatrix} x \\ y \end{pmatrix},$$

where

$$\tan \theta = \frac{\alpha_k^f - \alpha_k^i}{\alpha^f - \alpha^i}.$$

In this new system we expand the path  $y(x)$  in Fourier series

$$y(x) = \sum_k^N a_k \sin \left[ \frac{k\pi x}{x^f} \right] \quad (8)$$

and the action integral

$$S(L) = \frac{2^{3/2} B^{1/2}}{\hbar} \int_0^{x^f} \sqrt{V(x, y(x)) - E} dx$$

becomes a function of  $N$  variables  $a_k$ .

The path of minimum action satisfies the conditions

$$\frac{\partial S(L)}{\partial a_k} = \frac{2^{1/2}}{\hbar} \int_0^{x^f} \frac{\frac{\partial V}{\partial y} \sin\left(\frac{k\pi x}{x^f}\right)}{\sqrt{V(x, y(x)) - E}} dx = 0 \quad k = 1, \dots, N. \quad (9)$$

This nonlinear system of equations is solved by iterations starting from a guessed path. The initial set  $a_k^0$  is obtained by fitting the guess path with Eq. (9) by the least-squares method. Then at each iteration  $m$ , we increment the coefficients using the gradient descent method

$$a_k^{m+1} = a_k^m - c \frac{\partial S}{\partial a_k}$$

until convergence is attained

$$\sqrt{\sum_k \left( \frac{\partial S}{\partial a_k} \right)^2} < \delta.$$

50 to 100 iterations are usually enough.  $c$  is a small number adjusted by trial and error.

Consistency between the macroscopic and microscopic terms of  $E_{\text{def}}$  in Eq. (1) requires a proper choice of the parameters involved. It is usually attained by fitting the coefficients of the macroscopic energy to the known ground state masses. This choice may depend on the description of the nuclear shapes and on the parameters of the microscopic energy used. Since the present work is the first evaluation of the fission barriers using generalized Cassini ovals, it is necessary to test the stability of the results against existing macroscopic models.

There are two types of macroscopic models: 1) for nuclei with sharp surfaces (the standard LDM) and 2) for nuclei with diffused surfaces (the finite-range LDM). We will use parameter sets from each category.

The terms dependent on deformation are

$$E_{\text{def}}^{\text{LD}} = A^{2/3} \{ [B_{\text{surf}}(\text{shape}) - 1] a_s + \frac{Z^2}{A} [B_{\text{Coul}}(\text{shape}) - 1] a_c \}. \quad (10)$$

We will use this form to compare different sets ( $a_c$ ,  $a_s$ ), i.e., different existing models.

### III. NUMERICAL RESULTS

In this study, we will take into account  $\alpha_3$  (octupole) and  $\alpha_4$  (hexadecapole) deformation parameters in addition to  $\alpha_1$  (asymmetry of fragment masses) and  $\alpha$  (main fission elongation). Results are presented for the low energy fission of  $^{236}\text{U}$ .

A shortcoming of our approach is that only axially symmetric shapes are considered. It is known that nonaxiality lowers the mass symmetric first barrier but axiality is usually restored at the second barrier which in turn becomes mass-asymmetric [45–53]. It is also known that fission observables (such as cross sections) are mainly determined by the fission threshold energy (i.e., by the higher of the two barriers). As long as the second barrier is the highest (as in  $^{236}\text{U}$ ), neglecting nonaxiality is an acceptable approximation.

Even self-consistent approaches seem to agree with the above statement. Calculations using nuclear density functional theory beyond the second fission barrier [54] show no effect of nonaxiality for  $^{236}\text{U}$  when the octupole deformation is taken into account. The results of self-consistent covariant calculations are more ambiguous [55,56]. While the importance of the triaxial deformation on the inner barrier and that of the octupole deformation on the outer barrier are well confirmed [57], the outer barriers are found to be lower (by about 1 MeV) when triaxial deformations are included although it is not clear if the octupole is constrained or not.

#### A. Potential energy surfaces, paths, and barriers

In the lower part of Fig. 3, the potential energy of deformation, Eq. (1), is plotted from a spherical nucleus to the scission point ( $r_{\text{neck}} = 0$ ) in the plane ( $\alpha$ ,  $\alpha_1$ ). Then, in Fig. 4, the deformation energy is minimized, at each point, with respect to  $\alpha_4$ . On these PES, we calculate the most probable fission paths. Three static methods are used. Besides the line of minimum  $E_{\text{def}}$  values and the path of minimum action integral, the path of steepest descent is added for comparison. The

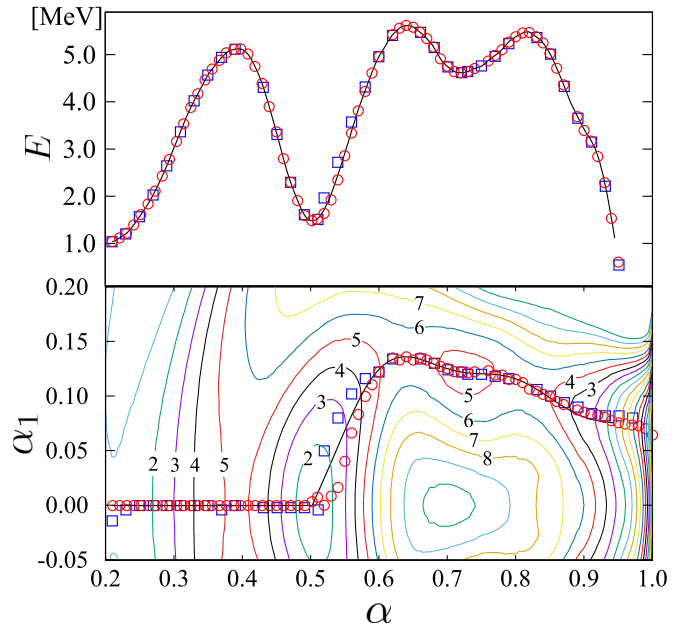


FIG. 3. Total deformation energy as a function of overall elongation ( $\alpha$ ) and mass asymmetry ( $\alpha_1$ ) for  $^{236}\text{U}$  between a sphere and the scission line. On it the fission path calculated in three different ways is drawn. The red circles represent the minimum energy, the blue squares follow the steepest descent, and the solid curve represents the path of minimum action (von Ritz). The fission barriers along each path are plotted in the upper part.

three derived paths are in good agreement. The corresponding fission barriers calculated along different fission paths are represented in the upper part of the figures. A perfect agreement between them is seen. So static fission barriers can be extracted unambiguously from PES calculations.

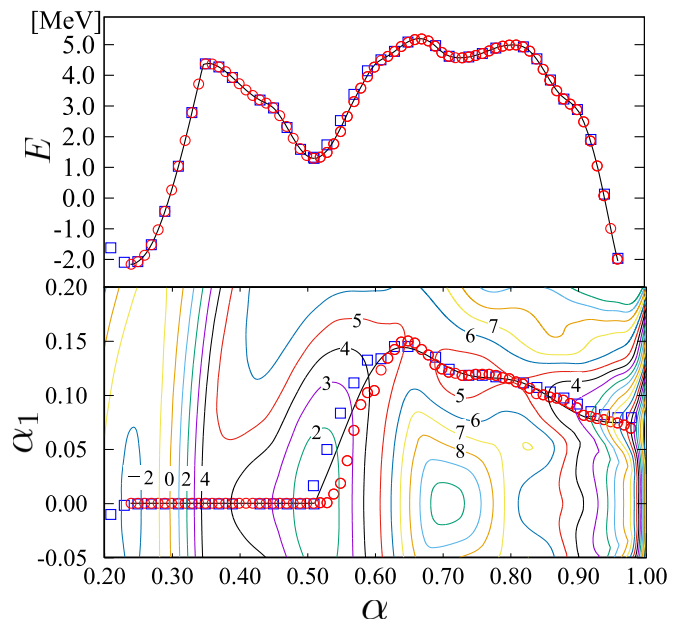


FIG. 4. The same as in Fig. 3 but with inclusion of ( $\alpha_4$ ) and minimization with respect to it.

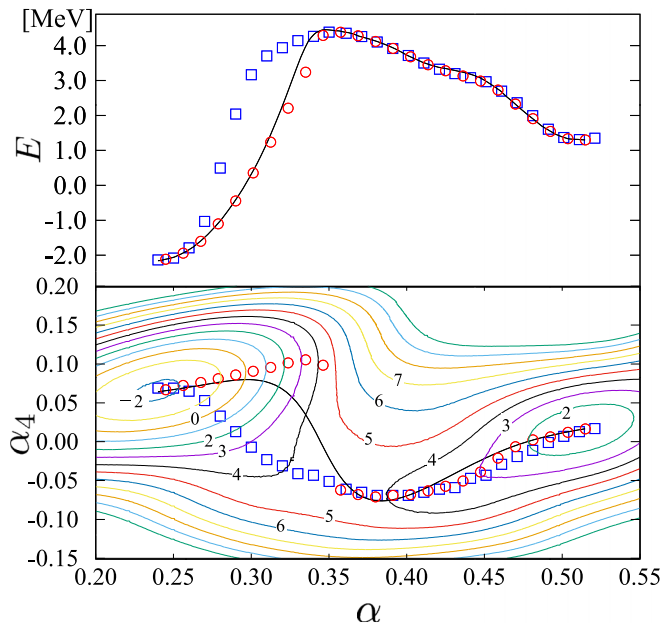


FIG. 5. Total deformation energy as a function of overall elongation ( $\alpha$ ) and hexadecapole ( $\alpha_4$ ) for  $^{236}\text{U}$  between the ground state and the second minimum. The points of minimum deformation energy (red circles), of steepest descent (blue squares), and the path of minimum action (solid black) are also shown. The fission barriers along each path are plotted in the upper part.

From the ground state ( $\alpha = 0.24$ ) to the second well ( $\alpha = 0.51$ ) the fission path stays along the  $\alpha_1 = 0$  line, i.e., the nucleus keeps its reflection symmetry. At larger elongations, the path goes into the mass asymmetry region reaching the second saddle point at  $\alpha = 0.64$  and  $\alpha_1 = 0.15$ . A triple-humped barrier can be observed in both figures, with the third barrier at about  $\alpha = 0.81$  and  $\alpha_1 = 0.11$  and an outer well of  $\approx 1$  MeV depth.

The existence of triple-humped fission barriers in light actinides has been documented both experimentally and theoretically [46–52]. The present calculations, using a shape parametrization suitable for extremely deformed (pronounced neck) nuclear configurations, can describe triple-humped barriers with only two shape parameters. However, as we will see in the following, the inclusion of the octupole deformation ( $\alpha_3$ ) makes the third minimum shallower and therefore unlikely to be experimentally observed in the case of  $^{236}\text{U}$ .

As compared with Fig. 3, Fig. 4 has a hidden dimension  $\alpha_4$ . To disclose the missing information, we show in Fig. 5 the results in the  $(\alpha_4, \alpha)$  plane between the ground state and the second minimum. This is where  $\alpha_4$  really matters since, although the inclusion of  $\alpha_4$  lowers  $E_{\text{def}}$  everywhere, this decrease is important only around the ground state. The resulting fission paths obtained by the three methods are also plotted.

The curve of minimum energy as a function of the main fission coordinate presents, at the first saddle, a shape transition that makes the fission path discontinuous. It is therefore not a path in the usual sense of a set of contiguous points. However, such a sharp decrease in the hexadecapole deformation along the trajectory of a fissioning nucleus in the multidimensional

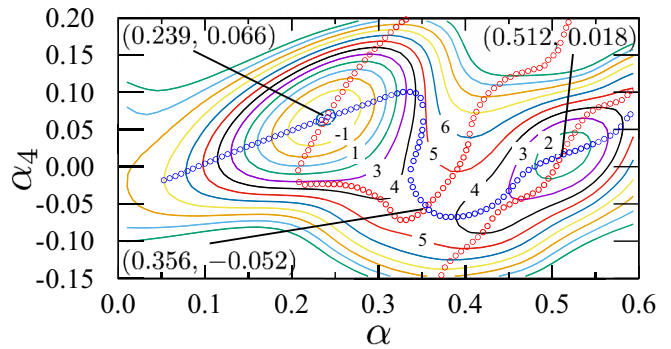


FIG. 6. Total deformation energy as a function of overall elongation ( $\alpha$ ) and hexadecapole ( $\alpha_4$ ) for  $^{236}\text{U}$  between the ground state and the second minimum. The lines corresponding to  $\frac{\partial E_{\text{def}}}{\partial \alpha} = 0$  (red) and  $\frac{\partial E_{\text{def}}}{\partial \alpha_4} = 0$  (blue) are superposed. Their intersection precisely defines the extreme points on the PES, i.e., the GS, the 1stB, and the 2ndM.

deformation space is physically possible since there is no discontinuity in energy. It is even possible to project on another axis, at an angle with  $\alpha$ , and make the discontinuity disappear. In addition, if we minimize the action integral we obtain a line that smoothly joins the two minima with the first saddle. Although the two paths are very different, the corresponding barriers are almost identical (see upper part). Therefore such discontinuities do not have dramatic consequences. The advantage of the von Ritz method is that it allows an easier localization of the top of the barrier.

The simplest exact way to find the extreme points is illustrated in Fig. 6. They are at the intersection of the lines corresponding to  $\frac{\partial E_{\text{def}}}{\partial \alpha} = 0$  and  $\frac{\partial E_{\text{def}}}{\partial \alpha_4} = 0$ . This is an original method worth to be studied further.

Discontinuities in the multidimensional PES have been extensively discussed both in the frame of a phenomenological model (finite number of shape parameters) [53] and a self-consistent model (automatic minimization in the nonconstrained degrees of freedom) [58,59] and methods to avoid them have been suggested. These studies concern complex discontinuities in the potential energy and not only in the nuclear shape. In the present study, however, only pure shape transitions that preserve the energy, are encountered. Moreover, the simple principle of stationary action, transforming a discontinuous trajectory into a continuous one, naturally smoothes out such transitions. In Fig. 7, the one-to-one correspondence between  $\alpha_1$  and the fragment-mass ratio is used to put the heavy fragment mass along the ordinate. The value of the light fragment mass along the valley towards scission is identical to the most probable experimental value ( $A_L = 96$ ). It is an ideal situation with no discontinuity along the fission path from the second minimum to the scission point. In this case the good agreement between the paths obtained by the two procedures (points of minimum energy and of minimum action) is not surprising.

Coming next is the inclusion of the octupole deformation  $\alpha_3$  together with  $\alpha$  and  $\alpha_1$ . It is worth mentioning that the fission fragment mass depends both on  $\alpha_1$  and on  $\alpha_3$ . In order to use  $A_F$  (an observable) on the vertical axis (like in Fig. 7),

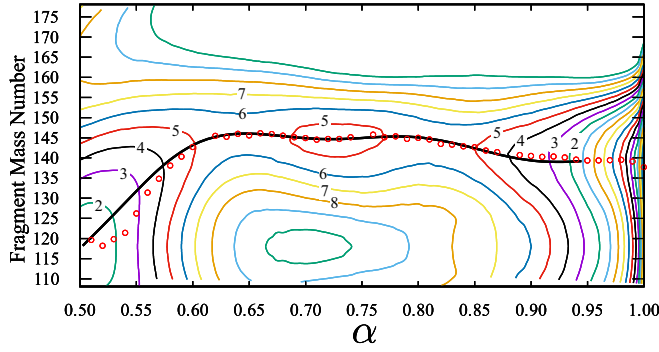


FIG. 7. Total deformation energy as a function of overall elongation ( $\alpha$ ) and fragment mass ( $A_F$ ) for  $^{236}\text{U}$  between the second minimum and the scission line.  $\alpha_4 = 0$ . The points of minimum deformation energy (red) and the path of minimum action (black) are also shown.

one needs to minimize  $E_{\text{def}}$  with respect to  $\alpha_1$  and  $\alpha_3$  for each point ( $\alpha$ ,  $A_F$ ).

The result is presented in the planes ( $\alpha$ ,  $A_F$ ) in Fig. 8. The plots cover the region from the second well to the scission line. The fission path is again discontinuous because of a shape transition (similar to the one encountered in Fig. 5) that occurs around the second barrier (i.e., at  $\alpha = 0.65$ ), namely a transition from  $A_F = 164$  to  $A_F = 142$ .

One can easily distinguish in Fig. 8 a third well (at  $\alpha = 0.72$ ,  $A_F = 135$  with  $E_3 = 4.3$  MeV) and a third barrier (at  $\alpha = 0.78$ ,  $A_F = 135$  with  $B_3 = 4.5$  MeV). The values of  $E_3$  and  $B_3$  are, respectively, 0.5 MeV and 1.0 MeV lower than the

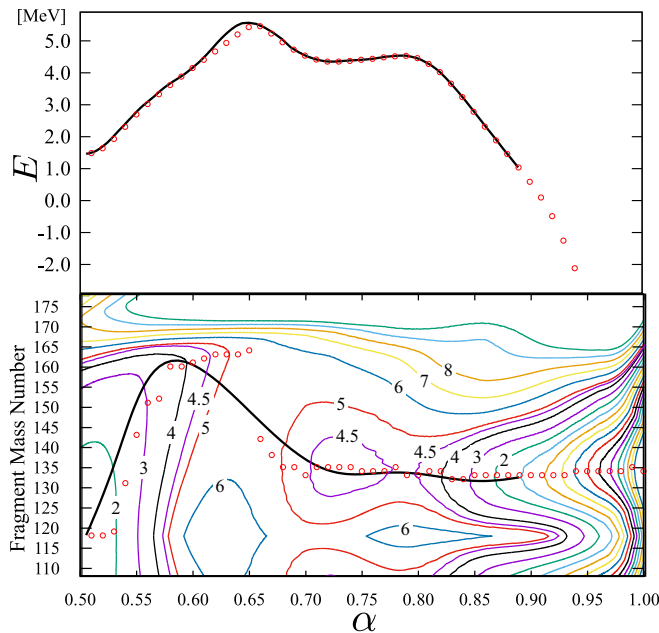


FIG. 8. Total deformation energy as a function of overall elongation ( $\alpha$ ) and fragment mass ( $A_F$ ) for  $^{236}\text{U}$  between second minimum and scission. At each point, the energy is minimized as a function of the octupole deformation  $\alpha_3$ . The points of minimum deformation energy (red) and the path of minimum action (black) are also shown.

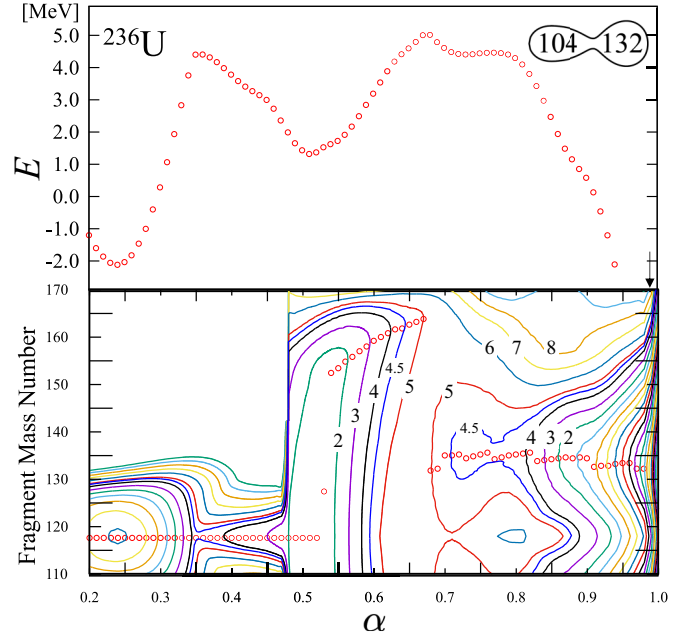


FIG. 9. The same as in Fig. 8 but with additional minimization on  $\alpha_4$ .

corresponding values from Fig. 3 obtained without inclusion of  $\alpha_3$ . Hence the octupole deformation plays a significant role beyond the second saddle. In this case, it lowers the third barrier making the third well extremely shallow.

In Fig. 8 there is another valley to scission that corresponds to symmetric mass division. This second valley is steeper than the asymmetric valley and the barrier leading to it is 1 MeV higher. There is however a non-negligible probability of populating it in a dynamical Langevin approach.

At this point, it is appropriate to comment on the fission modes that received much attention following the publication of the multi-modal random neck rupture model [60]. Using the generalized (five parameters) Lawrence [61] description of the nuclear shapes, it predicts several valleys on the PES leading to different scission configurations. Precise measurements [62–65], performed at JRC-Geel, of fragment mass and kinetic energy distributions in neutron induced fission of  $^{235}\text{U}$  and  $^{238}\text{U}$  at incident neutron energies from 1.2 to 5.8 MeV have been quantitatively explained in terms of two asymmetric and one symmetric (superlong) modes. Why do other parametrizations (like ours but not only) not reveal the second asymmetric valley? It is intriguing.

In principle, in a phenomenological model like ours, if the number of selected parameters is not enough or if we did not select the ones that are relevant for our problem, an additional shape parameter may considerably change the landscape of the PES invalidating the previous result. This does not seem to be the case in the present calculations. As compared with Fig. 8, in Fig. 9 we include an additional parameter ( $\alpha_4$ ) and minimize the deformation energy with respect to it. One sees no significant change in the PES from the second minimum until scission. This is an expected behavior for a well converged multipolar shape expansion.

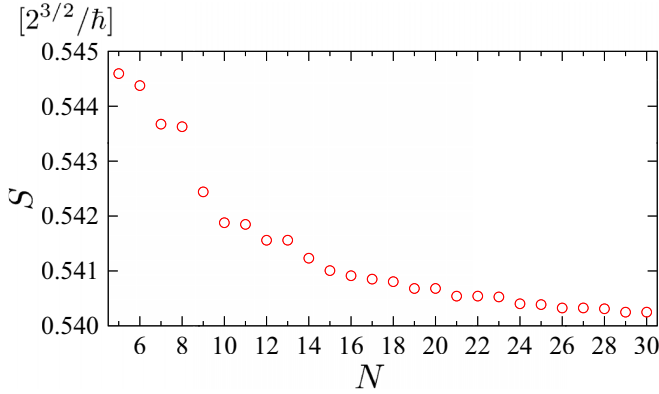


FIG. 10. Dependence of the minimum action integral  $S$  on the number of terms  $N$  in Eq. (9).

In conclusion the generalization of the Cassini ovals, Eq. (5), is an efficient parametrization for the sequence of shapes that a fissioning nucleus goes through. Practically  $(\alpha, \alpha_1$  and  $\alpha_3)$  are enough from the second minimum to the scission point.  $\alpha_4$  is important only from around the ground state till the second minimum. In the rest, it is used to verify that convergence has been attained.

### B. Input for the von Ritz method

The definition of the fission path as the one which leads to a minimum action integral is more physical than the determination of the path connecting the points of lowest deformation energy in the sense that the former is equivalent to the classical path. We analyze this method in more detail here. It has two inputs: an initial guess for this path, necessary to solve Eq. (10) and the number of terms  $N$  in the Fourier series (9). Figure 10 shows the dependence on  $N$ . Viewing the scale of  $S$  even  $N = 5$  gives enough precision. The minimum paths corresponding to three values of  $N$  are shown in Fig. 11. The differences are negligible.

So far, as initial trial path, we have taken the minimum energy points. To see the dependence of the minimum action path on this choice, a parabola connecting the inner and the outer points was also considered. Figure 12 shows that these

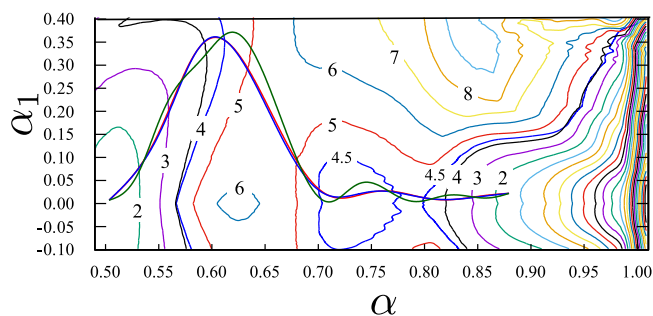


FIG. 11. Influence of the number of terms  $N$  in Eq. (9) on the minimum path.  $N = 7$  (red),  $N = 8$  (blue),  $N = 9$  (green). The PES is minimized with respect to  $\alpha_3$ .

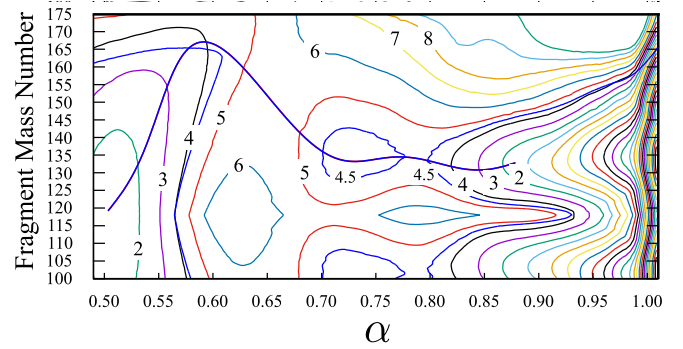


FIG. 12. Influence of the initial trial path (parabola or points of minimum deformation energy) on the minimum path.  $N = 5$ . The two paths are identical. The PES is minimized with respect to  $\alpha_3$ .

two choices (although very different) lead to the same path. This independence on the initial path is valid for any value of  $N$  (see Fig. 13). Therefore, our method to find the path that minimizes the action integral does not depend on the input.

### C. Calculation of the extreme points on the PES with different macroscopic models

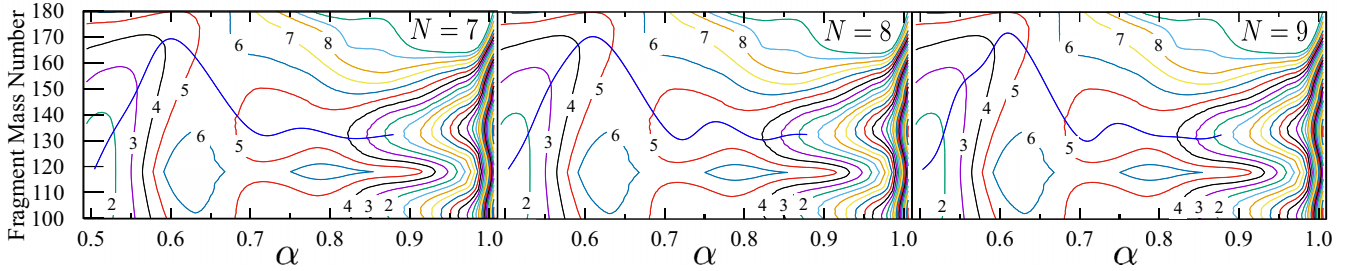
We now study the effect of the macroscopic model chosen to calculate  $E_{\text{def}}^{\text{LD}}$ . For this we use Eq. (11) in which the deformation dependent surface and Coulomb terms are characterized by the coefficients  $a_s$  and  $a_c$ . The five sets of values used are listed in Table I. The first four models consider sharp nuclear surfaces while the last uses a diffused surface. For this calculation, we restrict to the plane  $(\alpha, \alpha_1)$ , i.e., (overall elongation, mass asymmetry). (See Fig. 3 for an example of such a PES.) One should remember that, in a restricted space, the first minimum does not necessarily coincide with the ground state, i.e., it does not always have the lowest energy.

Table II contains the total energies [Eq. (1)] of the minima and of the saddles along the least energy path obtained with the five macroscopic models explored here. For the energies of the first minimum, the agreement is excellent. This is not surprising since in all models  $a_s$  and  $a_c$  are adjusted (together with other model parameters) mainly to the ground-state masses. Moreover compact configurations are well described by all shape parametrizations.

It is worth noticing that all models predict close-together positions for the extreme points in the plane  $(\alpha, \alpha_1)$  as seen in Table III. The second barrier, for instance, is always situated at  $\alpha = 0.638 \pm 0.002$  and  $\alpha_1 = 0.136 \pm 0.003$ . This shows that it is the microscopic term,  $\delta E(\text{shape})$ ,

TABLE I. Macroscopic parameters used for comparison.

Set	$a_s$	$a_c$	Ref.
(1)	16.390964	0.7053	[18]
(2)	16.0	0.7111	[17]
(3)	16.387185	0.720	[43]
(4)	16.159578	0.710	[66]
(5)	18.772828	0.744815	[51]

FIG. 13. The same as in Fig. 12 but for  $N = 7, 8,$  and  $9$ .

and not the macroscopic one,  $E_{\text{def}}^{\text{LD}}$  (shape), that determines these positions. The agreement of total energies is acceptable up to the second minimum and deteriorates as the elongation approaches the top of the LD barrier ( $\alpha > 0.65$ ) because, as seen in Fig. 14, different sets ( $a_s, a_c$ ) lead to different heights and shifted positions for this barrier.

So using parameters that reproduce ground-state masses does not guarantee reliable fission barriers, the outer one being the less precise. One reason is that only few barriers are included in the least-square fit. In Refs. [53,67], for instance, 28 barriers as compared with 1654 masses are used. So the barriers play a minor role in the fit. Moreover most terms in the mass formula are independent of deformation and the deformation window covered by nuclear ground states is very narrow.

In conclusion, the usual procedure cannot generate a unique deformation dependence of the total nuclear potential energy.

It would be better to use only deformation dependent terms and fit their coefficients to all existing data at large deformations, such as superdeformed ground states, shape isomers and other observables related to fission; not only fission barriers. It would also be safer to replace, when possible, the fit with theoretically estimated parameters. A new fitting procedure along the lines mentioned above requires a dedicated study that is outside the scope of the present work.

For applications where precise energies of the extreme points are needed, the best one can do, without redoing the fit, is to choose the Finite-Range Liquid Drop Model (FRLDM) [53] since it is based on a large number of masses and barriers.

The total deformation energy calculated self-consistently does not contain two separate terms, so the problem of consistency between macroscopic and microscopic contribu-

tions does not arise. However, the nucleon-nucleon effective interaction is usually chosen to reproduce ground state masses [68] and only rarely fission barriers [69].

#### IV. SUMMARY AND CONCLUSIONS

Calculations of PES as a function of four deformation parameters are performed, for the fission of  $^{236}\text{U}$ , in the frame of the microscopic-macroscopic model with a Cassini-oval description of the nuclear shapes involved.

The existence of a triple-humped barrier with a shallow third minimum in this nucleus is established. The octupole deformation plays an important role in the last stage of the fission process. It modifies the landscape and lowers the third minimum and the third barrier.

The fission paths are calculated on these PES in order to localize the minima and the saddles. Two definitions are used:

- (1) the points of lowest deformation energy  $E_{\text{def}}^{\text{min}}(\alpha_i)$  as a function of the main fission coordinate  $\alpha$ , and
- (2) the path in the deformation space  $L(\alpha_i)$  that corresponds to the minimum value of the action integral obtained by the von Ritz method.

TABLE III. Comparison of macroscopic energies,  $E_{\text{LD}}$  (MeV), and shape parameters  $\alpha, \alpha_1$  (next two lines) at the extreme points. The symbols M and B are for the minima and the barriers respectively.

Set	1stM	1stB	2ndM	2ndB	3rdM	3rdB
(1)	0.98	3.08	4.45	7.05	7.65	7.47
	0.208	0.396	0.502	0.640	0.720	0.816
	0.000	0.000	0.000	0.138	0.122	0.109
(2)	0.84	2.44	3.48	5.23	5.19	4.62
	0.210	0.391	0.509	0.636	0.765	0.800
	0.000	0.000	0.000	0.133	0.119	0.114
(3)	0.91	2.71	3.89	5.94	6.21	5.51
	0.209	0.393	0.507	0.637	0.744	0.809
	0.000	0.000	0.000	0.133	0.120	0.109
(4)	0.89	2.67	3.81	5.86	6.13	5.42
	0.209	0.393	0.504	0.637	0.744	0.810
	0.000	0.000	0.000	0.134	0.120	0.109
(5)	0.88	2.68	3.95	6.07	6.54	6.15
	0.209	0.391	0.504	0.637	0.725	0.813
	0.000	0.000	0.000	0.139	0.123	0.114

TABLE II. Comparison of total energies (with respect to the energy of the spherical liquid drop) at the extreme points in MeV. The symbols M and B are for the minima and the barriers, respectively.

Set	1stM	1stB	2ndM	2ndB	3rdM	3rdB
(1)	1.05	5.12	1.48	5.62	4.61	5.47
(2)	0.90	4.54	0.45	3.93	2.16	2.26
(3)	0.96	4.78	0.87	4.61	3.17	3.46
(4)	0.95	4.74	0.82	4.53	3.08	3.38
(5)	0.94	4.79	0.94	4.65	3.44	3.91

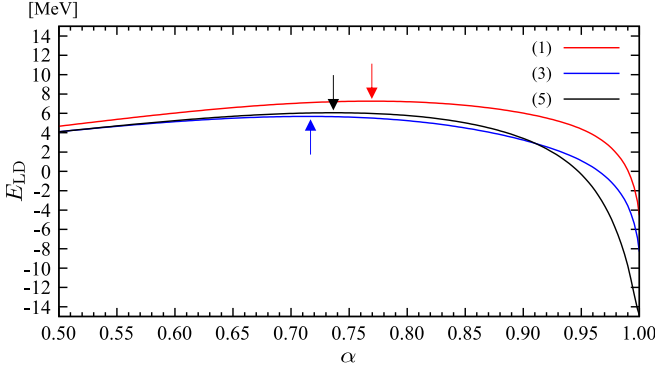


FIG. 14. The liquid-drop fission barrier for three sets of parameters ( $a_s$ ,  $a_c$ ). The arrows indicate the barrier tops.

The former may contain a sudden shape transition around the saddle point without a discontinuity in the value of  $E_{\text{def}}$ . In this case, the latter smoothly connects the branches before and after the transition. The two methods are consistent in the sense that they lead to the same fission barrier. The independence of the von Ritz method on its input (the initial trial path and the number of terms in the Fourier series) is demonstrated.

Finally, the dependence of the results on the choice of the LDM is calculated for five different models. It is found that the method largely used to fix the parameters ( $a_s$ ,  $a_c$ ) based on the experimental ground-state nuclear masses cannot uniquely predict the behavior at large deformations.

In conclusion, we developed a formalism to characterize the extremal points along the fission path using a description of nuclear shapes that is proper to the fission process. Four shape parameters are enough to provide the information needed for fundamental research and applications, in particular for the calculation of fission cross sections.

#### ACKNOWLEDGMENTS

We are grateful to Walter Furman and Yuri Kopach for their interest in this work and useful discussions. This work was supported by JST SPRING, Grant No. JPMJSP2150, and the Sasakawa Scientific Research Grant from the Japan Science Society. Numerical computations in this work were carried out at the Yukawa Institute Computer Facility and Cybermedia Center, Osaka University.

TABLE IV. Maximum quantum numbers and total number of states.

$\alpha$	$\omega_z [\hbar\omega]$	$\omega_\rho [\hbar\omega]$	$(n_z)_{\text{max}}$	$(n_\rho)_{\text{max}}$	total number
0.205	0.875	1.069	19	7	1011
0.985	0.425	1.534	39	5	1043

#### APPENDIX: NUMERICAL PARAMETERS; FREQUENCIES AND NUMBER OF STATES IN THE BASIS; NUMBER OF INTEGRATION POINTS

The Hamiltonian is diagonalized by the wave functions of the deformed harmonic oscillator in cylindrical coordinates. By adapting the frequencies of the deformed harmonic oscillator to the actual fission shape [70], we keep the number of basis states relatively constant as a function of  $\alpha$  (as seen in Table IV). The frequencies  $\omega_\rho$  and  $\omega_z$  depending on the Cassini parameters are obtained by the equations

$$\{(\hbar\omega_\rho)^2 \hbar\omega_z\}^{1/3} = \hbar\omega = 41A^{-1/3}, \quad (\text{A1})$$

$$\frac{\omega_\rho^2}{\omega_z^2} = \frac{\langle z^2 \rangle}{\langle \rho^2 \rangle}$$

$$= \frac{\int_{-1}^1 (\bar{z} - \bar{z}_{\text{c.m.}})^2 \bar{\rho}^2 \frac{d\bar{z}}{dx} dx}{\int_{-1}^1 \bar{\rho}^4 \frac{d\bar{z}}{dx} dx}. \quad (\text{A2})$$

In the present calculations, we adopt states that satisfy the condition  $E_{n_z, n_\rho, \lambda} < 18.5\hbar\omega$ , where the single-particle energy of the deformed harmonic oscillator  $E_{n_z, n_\rho, \lambda}$  is given as

$$E_{n_z, n_\rho, \lambda} = \left(n_z + \frac{1}{2}\right)\hbar\omega_z + (2n_\rho + \lambda + 1)\hbar\omega_\rho. \quad (\text{A3})$$

Table IV contains information of the basis in two cases:  $\alpha = 0.205$  (ground state) and  $\alpha = 0.985$  (scission). For simplicity,  $\alpha_n = 0$  are used. The maximum quantum numbers and the total number of states. As can be seen,  $(n_z)_{\text{max}}$  increases when the nucleus is elongated.

Concerning the number of integration points in the calculation of surface and Coulomb energies, we divided the domain  $[-1, +1]$  of the Cassini coordinate  $x$  into four equal parts. In each part, we performed a Legendre integral of 20 points. Then we summed the four results. In this way the energies have six exact digits.

- [1] N. Carjan, F. A. Ivanyuk, and Yu. Oganessian, Pre-scission model predictions of fission fragment mass distributions for super-heavy elements, *Nucl. Phys. A* **968**, 453 (2017).
- [2] G. Scamps and C. Simenel, Impact of pear-shaped fission fragments on mass-asymmetric fission in actinides, *Nature (London)* **564**, 382 (2018).
- [3] K. Mahata, C. Schmitt, Shilpi Gupta, A. Shrivastava, G. Scamps, and K.-H. Schmidt, Evidence for the general dominance of proton shells in low-energy fission, *Phys. Lett. B* **825**, 136859 (2022).
- [4] G. Scamps and C. Simenel, Effect of shell structure on the fission of sub-lead nuclei, *Phys. Rev. C* **100**, 041602(R) (2019).

- [5] A. S. Davydov, *Excited States of Atomic Nuclei* (in Russian) (Atomizdat, Moscow, 1967).
- [6] E. Sh. Sukhovitskiĭ and Yu. V. Porodzinskiĭ, 238U Coupled-Channels Optical Model Calculations: Search for collective level structure saturating coupling, *Proceedings of 9th International Symposium on Capture Gamma-Ray Spectroscopy and Related Topics* (Budapest, Hungary, 1996), Vol. 1, p. 335.
- [7] E. Sh. Sukhovitskiĭ and Yu. V. Porodzinskiĭ, *Sov. J. Nucl. Phys.* **54**, 570 (1991).
- [8] Yu. V. Porodzinskiĭ and E. Sh. Sukhovitskiĭ, Analysis of neutron scattering by even-even nuclei with allowance for dynamical octupole deformations, *Phys. At. Nucl.* **59**, 228 (1996).

- [9] E. Sh. Sukhovitskiĭ, S. Chiba, O. Iwamoto, and Yu. V. Porodzinskiĭ, Nucleon interaction with  $^{12}\text{C}$  studied by the soft-rotator model and a limit on the charge-symmetry breaking in the nuclear mean field, *Nucl. Phys. A* **640**, 147 (1998).
- [10] T. Tamura, Analyses of the scattering of nuclear particles by collective nuclei in terms of the coupled-channel calculation, *Rev. Mod. Phys.* **37**, 679 (1965).
- [11] T. Kawano, N. Fujikawa, and Y. Kanda, Evaluation of  $^{238}\text{U}$  inelastic scattering cross section, Technical Report JAERI-M-94-019, INDC(JPN)-169, Japan Atomic Energy Research Institute, Ibaraki-ken, Japan (1994).
- [12] V. M. Maslov, Yu. V. Porodzinskij, N. A. Tetereva, M. Baba, and A. Hasegawa, Excitation of octupole, beta- and gamma-vibration band levels of  $^{238}\text{U}$  by inelastic neutron scattering, *Nucl. Phys. A* **764**, 212 (2006).
- [13] P. Romain, B. Morillon, and H. Duarte, Bruyères-le-Châtel neutron evaluations of actinides with the TALYS code: The fission channel, *Nucl. Data Sheets* **131**, 222 (2016).
- [14] J. M. Quesada, R. Capote, E. Sh. Soukhovitskiĭ, and S. Chiba, Rotational-vibrational description of nucleon scattering on actinide nuclei using a dispersive coupled-channel optical model, *Nucl. Data Sheets* **118**, 270 (2014).
- [15] E. Sh. Soukhovitskiĭ, R. Capote, J. M. Quesada, S. Chiba, and D. S. Martyanov, Nucleon scattering on actinides using a dispersive optical model with extended couplings, *Phys. Rev. C* **94**, 064605 (2016).
- [16] V. M. Strutinsky, Shell effects in nuclear masses and deformation energies, *Nucl. Phys. A* **95**, 420 (1967).
- [17] V. Pashkevich, On the asymmetric deformation of fissioning nuclei, *Nucl. Phys. A* **169**, 275 (1971).
- [18] V. Pashkevich, Prescission shapes of symmetrically fissioning very heavy nuclei, *Nucl. Phys. A* **477**, 1 (1988).
- [19] N. Carjan, F. Ivanyuk, Yu. Oganessian, and G. Ter-Akopian, Fission of transactinide elements described in terms of generalized Cassinian ovals: Fragment mass and total kinetic energy distributions, *Nucl. Phys. A* **942**, 97 (2015).
- [20] K. T. R. Davies, R. A. Managan, J. R. Nix, and A. J. Sierk, Rupture of the neck in nuclear fission, *Phys. Rev. C* **16**, 1890 (1977).
- [21] S. Cwiok, P. Rozmej, A. Sobiczewski, and Z. Patyk, Two fission modes of the heavy fermium isotopes, *Nucl. Phys. A* **491**, 281 (1989).
- [22] S. Pal, G. Chaudhuri, and J. Sadhukhan, The role of neck degree of freedom in nuclear fission, *Nucl. Phys. A* **808**, 1 (2008).
- [23] Z.-H. Liu and J.-D. Bao, Role of the coupling between neck and radial degrees of freedom in evolution from dinucleus to mononucleus, *Phys. Rev. C* **83**, 044613 (2011).
- [24] G. G. Adamian, N. V. Antonenko, and H. Lenske, Role of the neck degree of freedom in cold fusion reactions, *Phys. Rev. C* **91**, 054602 (2015).
- [25] K. Pomorski, B. Nerlo-Pomorska, J. Bartel, and C. Schmitt, Fission fragment mass and total kinetic energy distributions of spontaneously fissioning plutonium isotopes, *EPJ Web Conf.* **169**, 00016 (2018).
- [26] A. Zdeb, M. Warda, and L. M. Robledo, Description of the multidimensional potential-energy surface in fission of  $^{252}\text{Cf}$  and  $^{258}\text{No}$ , *Phys. Rev. C* **104**, 014610 (2021).
- [27] M. Brack, J. Damgaard, A. S. Jensen, H. C. Pauli, V. M. Strutinsky, and C. Y. Wong, Funny Hills: The Shell-Correction Approach to Nuclear Shell Effects and Its Applications to the Fission Process, *Rev. Mod. Phys.* **44**, 320 (1972).
- [28] R. Capote, N. Carjan, and S. Chiba, Scission neutrons for U, Pu, Cm, and Cf isotopes: Relative multiplicities calculated in the sudden limit, *Phys. Rev. C* **93**, 024609 (2016).
- [29] E. Rost, Proton shell-model potentials for lead and the stability of superheavy nuclei, *Phys. Lett. B* **26**, 184 (1968).
- [30] P. Möller and J. R. Nix, Nuclear pairing models, *Nucl. Phys. A* **536**, 20 (1992).
- [31] W. D. Myers and W. J. Swiatecki, Anomalies in nuclear masses, *Ark. Fys.* **36**, 343 (1967).
- [32] F. Garcia, O. Rodriguez, J. Mesa, J. D. T. Arruda-Neto, V. P. Likhachev, E. Garrote, R. Capote, and F. Guzman, BARRIER code: Calculation of fission barriers, *Comput. Phys. Commun.* **120**, 57 (1999).
- [33] N. Carjan, F. Ivanyuk, and V. Pashkevich, Cassini-oval description of the energy balance at scission during  $^{235}\text{U}(n_{th}, f)$ , *Phys. Procedia* **31**, 66 (2012).
- [34] V. M. Strutinsky, N. Ya. Lyashchenko, and N. A. Popov, Symmetrical shapes of equilibrium for a liquid drop model, *Nucl. Phys.* **46**, 639 (1963).
- [35] U. Mosel and H. W. Schmitt, Fragment-shell influences in nuclear fission, *Phys. Rev. C* **4**, 2185 (1971).
- [36] P. Möller, Odd-multipole shape distortions and the fission barriers of elements in the region  $84 \leq z \leq 120$ , *Nucl. Phys. A* **192**, 529 (1972).
- [37] H. C. Pauli and T. Ledergerber, *Proceedings of the Third IAEA Symposium on the Physics and Chemistry of Fission*, Rochester, NY, 1973 (IAEA, Vienna, 1974), Vol. I, p. 463.
- [38] W. Stocker, J. Bartel, J. R. Nix, and A. J. Sierk, Anomaly in the nuclear curvature energy, *Nucl. Phys. A* **489**, 252 (1988).
- [39] A. Mamdouh, J. M. Pearson, M. Rayet, and F. Tondeur, Large-scale fission-barrier calculations with the ETFSI method, *Nucl. Phys. A* **644**, 389 (1998).
- [40] S. Goriely, F. Tondeur, and J. M. Pearson, A Hartree-Fock nuclear mass table, *At. Data Nucl. Data Tables* **77**, 311 (2001).
- [41] M. Samyn, S. Goriely, and J. M. Pearson, Further explorations of Skyrme-Hartree-Fock-Bogoliubov mass formulas. V. Extension to fission barriers, *Phys. Rev. C* **72**, 044316 (2005).
- [42] B. B. Back, O. Hansen, H. C. Britt, and J. D. Garrett, Fission of doubly even actinide nuclei induced by direct reactions, *Phys. Rev. C* **9**, 1924 (1974).
- [43] B. B. Back, H. C. Britt, O. Hansen, B. Leroux, and J. D. Garrett, Fission of odd-A and doubly odd actinide nuclei induced by direct reactions, *Phys. Rev. C* **10**, 1948 (1974).
- [44] H. C. Britt, *Proceedings of the 4th IAEA Symposium on the Physics and Chemistry of Fission*, Julich, 1979 (IAEA, Vienna, 1980), Vol. I, p. 3.
- [45] H. C. Pauli, On the shell model and its application to the deformation energy of heavy nuclei, *Phys. Rep.* **7**, 35 (1973).
- [46] J. Blons, R. Fabbro, C. Mazur, D. Paya, M. Ribrag, and Y. Patin, High resolution fission probabilities for  $^{229,230,232}\text{Th}(d, pf)$  and  $^{233,236}\text{U}(d, pf)$  reactions, *Nucl. Phys. A* **477**, 231 (1988).
- [47] J. Blons, A third minimum in the fission barrier, *Nucl. Phys. A* **502**, 121 (1989).
- [48] M.J. López Jiménez, B. Morillon, and P. Romain, Bruyères-le-Châtel neutron evaluations of actinides with the TALYS Code: The fission channel, *Ann. Nucl. Energy* **32**, 195 (2005).
- [49] M. Sin, R. Capote, A. Ventura, M. Herman, and P. Oblozinsky, Fission of light actinides:  $^{232}\text{Th}(n,f)$  and  $^{231}\text{Pa}(n,f)$  reactions, *Phys. Rev. C* **74**, 014608 (2006).

- [50] M. Sin, R. Capote, M. W. Herman, and A. Trkov, Modelling Neutron-induced Reactions on  $^{232-237}\text{U}$  from 10 keV up to 30 MeV, *Nucl. Data Sheets* **139**, 138 (2017).
- [51] T. Ichikawa, P. Möller, and A. J. Sierk, Character and prevalence of third minima in actinide fission barriers, *Phys. Rev. C* **87**, 054326 (2013).
- [52] P. Jachimowicz, M. Kowal, and J. Skalski, Eight-dimensional calculations of the third barrier in  $^{232}\text{Th}$ , *Phys. Rev. C* **87**, 044308 (2013).
- [53] P. Möller, A. J. Sierk, T. Ichikawa, A. Iwamoto, R. Bengtsson, H. Uhrenholt, and S. Aberg, Heavy-element fission barriers, *Phys. Rev. C* **79**, 064304 (2009).
- [54] C. Ling, C. Zhou, and Y. Shi, Fission barriers of actinide nuclei with nuclear density functional theory: Influence of the triaxial deformation, *Eur. Phys. J. A* **56**, 180 (2020).
- [55] B.-N. Lu, E.-G. Zhao, and S.-G. Zhou, Potential energy surfaces of actinide nuclei from a multidimensional constrained covariant density functional theory: Barrier heights and saddle point shapes, *Phys. Rev. C* **85**, 011301(R) (2012).
- [56] B.-N. Lu, J. Zhao, E.-G. Zhao, and S.-G. Zhou, Multidimensionally-constrained relativistic mean-field models and potential-energy surfaces of actinide nuclei, *Phys. Rev. C* **89**, 014323 (2014).
- [57] B.-N. Lu, J. Zhao, E.-G. Zhao, and S.-G. Zhou, Fission barriers from multidimensionally-constrained covariant density functional theories, *EPJ Web Conf.* **163**, 00034 (2017).
- [58] N. Dubray and D. Regnier, Numerical search of discontinuities in self-consistent potential energy surfaces, *Comput. Phys. Commun.* **183**, 2035 (2012).
- [59] N.-W. T. Lau, R. N. Bernard, and C. Simenel, Smoothing of one- and two-dimensional discontinuities in potential energy surfaces, *Phys. Rev. C* **105**, 034617 (2022).
- [60] U. Brosa, S. Grossmann, and A. Müller, Nuclear scission, *Phys. Rep.* **197**, 167 (1990).
- [61] J. N. P. Lawrence, Static fission-barrier calculations of a two-parameter liquid drop, *Phys. Rev.* **139**, B1227 (1965).
- [62] H.-H. Knitter, F.-J. Hamsch, C. Budtz-Jørgensen, and J. P. Theobald, Three exit channels in the fission of  $^{235}\text{U}(n, f)$ , *Z. Naturforsch. A* **42**, 786 (1987).
- [63] P. Siegler, F.-J. Hamsch, S. Oberstedt, and J. P. Theobald, Fission modes in the compound nucleus  $^{238}\text{Np}$ , *Nucl. Phys. A* **594**, 45 (1995).
- [64] S. Oberstedt, F.-J. Hamsch, and F. Vives, Fission-mode calculations for  $^{239}\text{U}$ , a revision of the multi-modal random neck-rupture model, *Nucl. Phys. A* **644**, 289 (1998).
- [65] F. Vives, F.-J. Hamsch, H. Bax, and S. Oberstedt, Investigation of the fission fragment properties of the reaction  $^{238}\text{U}(n, f)$  at incident neutron energies up to 5.8 MeV, *Nucl. Phys. A* **662**, 63 (2000).
- [66] R. Capote, (private communication).
- [67] P. Möller, J. R. Nix, W. D. Myers, and W. J. Swiatecki, Nuclear ground-state masses and deformations, *At. Data Nucl. Data Tables* **59**, 185 (1995).
- [68] M. Samyn, S. Goriely, Microscopic HFB fission barriers for r-process nucleosynthesis, *Nucl. Phys. A* **758**, 659 (2005).
- [69] J. Bartel, P. Quentin, M. Brack, C. Guet, and H.-B. Hakansson, Towards a better parametrisation of Skyrme-like effective forces: A critical study of the SkM force, *Nucl. Phys. A* **386**, 79 (1982).
- [70] J. Damgaard, H. C. Pauli, V. V. Pashkevich, and V. M. Strutinsky, A method for solving the independent-particle Schrödinger equation with a deformed average field, *Nucl. Phys. A* **135**, 432 (1969).